Use of wind pressure coefficients to simulate natural ventilation and building energy for isolated and surrounded buildings

Xiaoxiong Xie [a], Zhiwen Luo [a,b,*], Sue Grimmond [c], Lewis Blunn [c]

[a] *School of the Built Environment, University of Reading, United Kingdom*
[b] *Welsh School of Architecture, Cardiff University, United Kingdom*
[c] *Department of Meteorology, University of Reading, United Kingdom*

A R T I C L E   I N F O

Keywords:
Wind pressure coefficient
Natural ventilation
Building energy simulation
Urban climate
Overheating

A B S T R A C T

Wind pressure coefficients (C_p) are critical inputs to building energy simulations. Given differences in the free stream wind speed height two categories exist: (1) C_{pr} (reference height) and (2) C_{pl} (local opening height). Additionally, C_p data are influenced by the vertical wind profile which is modified by surrounding buildings. However, these dependencies are often overlooked in building energy simulations (BES). We identified three potential biases from the incorrect use of C_p: (1) C_{pr} is used alongside the wind speed at opening height rather than reference height (where C_{pr} is defined); (2) C_{pr} is used with wind profiles that are different from the wind tunnel experiment or CFD simulation used to derive C_{pr}; and, (3) C_p is used along with the 'disturbed' urbanised wind speed instead of the 'undisturbed' free stream wind speed. In this study, we quantify the resulting biases from using C_p data incorrectly by assessing impacts on the resulting ventilation rate, indoor overheating risks and cooling energy saving with EnergyPlus for Shanghai's climate. Modifications to the use of C_p are proposed to improve simulation accuracy. Results show biases mostly exceeding the ±10% limit of ASHRAE-14 in all scenarios analysed. Differences are up to −19.0% for natural ventilation rate, 13.2% for indoor overheating degree hours and −14.0% for cooling energy saving, with such errors being larger during heatwave periods. Our study could provide useful guidance for researchers to carry out wind-driven natural ventilation study and estimate indoor overheating risk and energy consumption with better accuracy.

$$C_{pl}(z) = \frac{P_w(z)}{0.5 \, \rho \, U_{free}^2(z)} \tag{2}$$

1. Introduction

Wind pressure coefficients (C_p) are key inputs for natural ventilation calculation in building energy simulations (BES) and multi-zone airflow models (e.g. AirflowNetwork (AFN) in EnergyPlus (EnergyPlus-AFN) [1], MacroFlo in IES-VE [2], CONTAM and COMIS linkages with TRNSYS [3]). C_p is the nondimensional ratio of wind pressure on the building surface to the dynamic pressure in the upstream undisturbed flow [4] but is defined differently depending on the height of free stream dynamic pressure [5]:

$$C_{pr}(z) = \frac{P_w(z)}{0.5 \, \rho \, U_{free}^2(H)} \tag{1}$$

where H is a *reference* height (m, building roof/eave height), or alternatively the *local* opening height z (m) is used [5]:

where $P_w(z)$ is the wind pressure (Pa) measured on the building facet at height z (m), U_{free} is the wind speed (m s^{-1}) in the upstream undisturbed flow at H or z, and ρ is the outdoor air density (kg m^{-3}) which is assumed constant. Typically, C_p is calculated as the average value across the entire building facet facing the flow (i.e. surface mean).

C_p is widely applied in studies of natural ventilation potential [6–9], cooling energy savings [10–13], indoor thermal comfort and overheating [14–17], and other applications like the solar chimney [18] and windcatcher [19]. Commonly the C_p data sources used in BES (Table 1) are from Ref. [21]: primary sources (e.g., full-scale experiments, wind tunnel experiments and CFD simulations for a specific building of interest); and secondary sources (e.g. databases with generic building archetypes derived often from wind tunnel experiments). In databases (Table 1), C_{pr} rather than C_{pl} data are provided and are the default values used in BES.

Nomenclature

A	Opening area (m^2)
C_d	Discharge coefficient of the opening
C_p	Wind pressure coefficient
C_{pl}	Wind pressure coefficient based on the (local) opening height
C_{pr}	Wind pressure coefficient based on the (reference) roof height
H	Roof height (m)
q_w	Wind-driven ventilation rate (m^3 s^{-1})
P_w	Wind pressure (Pa)
U	Wind speed (m s^{-1})
z	Opening height (m)

α	Wind profile exponent
δ	Height where a constant mean gradient wind speed is assumed to occur (m)
$λ_P$	Plan area fraction
ρ	Outdoor air density (kg m^{-3})
subscripts	
ref	Reference in the wind tunnel experiment
EP	EnergyPlus
free	Free stream wind
met	Reference in the meteorological observation site
r	Undisturbed rural wind
u	Disturbed urbanised wind
WT	Wind tunnel

Table 1

Summary of commonly used databases (DB#) of wind pressure coefficients (C_p) in building energy simulations (BES) either using reference height (C_{pr}) or the local height (C_{pl}). $\overline{C_{pr}}$ and $\overline{C_{pl}}$ refer to surface averaged C_{pr} and C_{pl} data, respectively. *$\overline{C_{pl}}$ data are also calculated but not used in ASHRAE *Handbook of Fundamentals* [20] and EnergyPlus [1]. In places information is not given (NG). Examples of where the data source are used in a BES tool as a default are given. Modified after Cóstola et al. [21].

DB#	C_p Source	Type	Wind profiles in wind tunnel experiments	Sheltering effects	BES Default
1	Akins et al. [5]	$\overline{C_{pr}}$ and $\overline{C_{pl}}$*	Provided	Isolated	EnergyPlus for high-rise buildings
2	AIVC [22]	$\overline{C_{pr}}$	NG	Isolated, semi-exposed or sheltered ($λ_P$ are not given)	IES-VE and DesignBuilder [23]
3	Swami an Chandra [24]	$\overline{C_{pr}}$	NG	Isolated, correction coefficients for ventilation rate	EnergyPlus for low-rise buildings
4	TPU [25]	$\overline{C_{pr}}$	Provided	$λ_P$ from 0.1 to 0.6	Used as external source

C_p data, together with the reference wind conditions, are regarded as the major sources of uncertainties in multi-zone airflow models [26,27]. Therefore, applying C_p data correctly is important for more accurate estimation of natural ventilation rates. C_p data are dependent on many factors including the height of free stream dynamic pressure measured and the vertical wind profile which is modified by the surrounding buildings [22,24]. However, these dependencies are often overlooked in BES, which could cause biases. Here we focus on EnergyPlus, as it is one of the most widely used open-source BES tools. Our aim is to critically explore potential biases of EnergyPlus-AFN simulation in three comparative C_p application scenarios (Fig. 1).

Scenario 1: In EnergyPlus the surface averaged C_{pr} ($\overline{C_{pr}}$) data are usually used with wind speed at the opening height $U_{free}(z)$. This is inconsistent (Eq. (1) cf. Eq. (2)) and can cause biases since $U_{free}(z)$ should be used with the surface averaged C_{pl} ($\overline{C_{pl}}$) (Fig. 1a). EnergyPlus options allow the use of either provided [5,24] or user-supplied C_p data. In the latter case, the user also needs to indicate the height the C_p values are for (i.e., opening or reference), with the EnergyPlus default (i.e., if not modified) being the opening height [28]. If the provided default C_p values are used, the opening height will be used (not explicitly stated in Ref. [28] but found in the source code [29] and mentioned by Refs. [13, 30,31]). Hence, the provided $\overline{C_{pr}}$ value is used with wind speed at the opening height (z) instead of the reference roof height (H). This inconsistency between $\overline{C_{pr}}$ and freestream wind speed will cause biases in the wind pressure calculations if not corrected. Given this, we review current studies for choosing C_p if modelling natural ventilation in buildings using EnergyPlus-AFN (Table 2). Typically, if the detailed C_p settings are not mentioned, the supplied default $\overline{C_{pr}}$ values are assumed to be used.
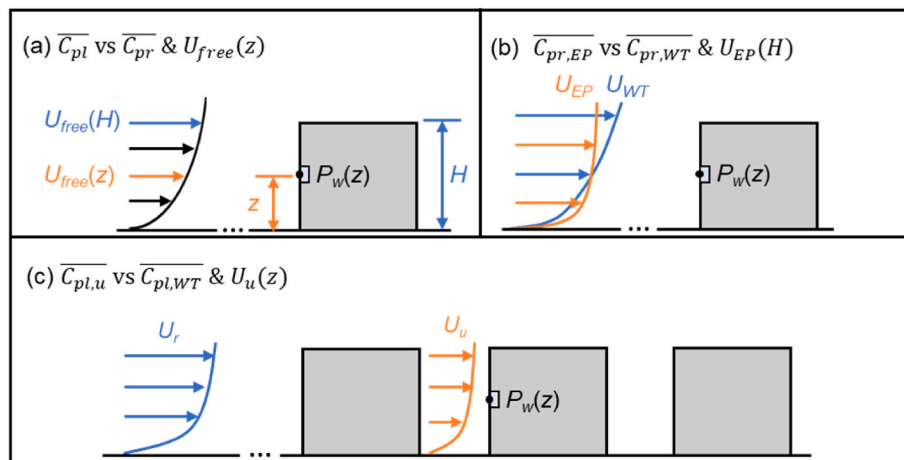

Fig. 1. Three scenarios (Section 1) to determine wind pressure coefficients (C_p) all assume they are surface-averaged ($\overline{C_{pl}}$ or $\overline{C_{pr}}$) but with different wind profiles (U): (a) *Scenario 1* are calculated with free stream wind speed at the opening height ($U_{free}(z)$), (b) *Scenario 2:* $\overline{C_{pr}}$ is derived from wind tunnel (WT) wind profile ($\overline{C_{pr,WT}}$) or from the EnergyPlus (EP) building energy simulation ($\overline{C_{pr,EP}}$); and (c) *Scenario 3:* $\overline{C_{pl}}$ is based on disturbed urbanised (u) wind speed ($\overline{C_{pl,u}}$) rather than an undisturbed free stream wind speed ($\overline{C_{pl,WT}}$).

Table 2

Summary of types of C_p data and wind speed height used in EnergyPlus and Airflow Network (AFN) studies. All C_p values are surface averaged values. Following [21], sources are either primary (1°) from wind tunnel (WT) experiments and computational fluid dynamics (CFD) simulations, or secondary (2°) from published databases (DB, with references to Table 1 indicated by #) or analytical tools for generic building archetypes. EnergyPlus-AFN studies that do not indicate the C_p method used, are assumed to use pre-provisioned C_{pr} values with wind speed at the opening height z. H refers to the reference building height. Sometimes information is not given (NG).

Reference	C_p		$\overline{C_{pr}}$ or $\overline{C_{pl}}$	Free stream wind speed height
	Source	Type		
Botti et al. [32]	2°	DB#3	$\overline{C_{pr}}$	z
Bre and Gimenez [33]	1°	CFD	$\overline{C_{pr}}$	H
Guo et al. [34]	1°	CFD	NG	NG
Toesca et al. [31]	2°	UrbaWind [35]	$\overline{C_{pr}}$	H
Dogan and Kastner [36]	1°, 2°	CFD, DB#3	$\overline{C_{pr}}$	z
Saif et al. [37]	2°	DB#2	$\overline{C_{pr}}$	NG
Sakiyama et al. [38]	2°	DB#3	$\overline{C_{pr}}$	z
Song et al. [39]	1°	WT	$\overline{C_{pl}}$	NG
Albuquerque et al. [40]	1°	CFD	$\overline{C_{pr}}$	H
Raji et al. [41]	1°	WT	NG	NG
Sadeghi et al. [19]	1°	WT	$\overline{C_{pr}}$	NG
Bayraktar and Ok [42]	1°	WT	NG	NG
Belmans et al. [43]	1°	CFD	$\overline{C_{pl}}$	z
Gimenez et al. [30]	1°	CFD	$\overline{C_{pr}}$	z
Kim et al. [44]	2°	DB#3	$\overline{C_{pr}}$	z
Short et al. [45]	1°	CFD	NG	NG
Southall [46]	2°	DB#3	$\overline{C_{pr}}$	z
Van Nguyen and De Troyer [47]	2°	C_p Generator [48]	$\overline{C_{pr}}$	NG
Bre et al. [49]	2°	DB#3	$\overline{C_{pr}}$	z
Sorgato et al. [50]	2°	C_p Generator [48]	$\overline{C_{pr}}$	NG
Belleri et al. [27]	1°	WT	NG	NG
Ramponi et al. [12]	1°	WT	$\overline{C_{pr}}$	NG
Joe et al. [51]	1°	CFD	$\overline{C_{pr}}$	NG
Schulze and Eicker [13]	2°	DB#2	$\overline{C_{pr}}$	z
You et al. [52]	1°	CFD	$\overline{C_{pr}}$	NG
Carrilho Da Graça et al. [53]	1°	CFD	NG	NG
Olsen and Chen [54]	1°	CFD	$\overline{C_{pr}}$	NG

Of the studies stating the C_p settings (fully or partly), only four [31,33,40,43] of 27 (Table 2) use the correct combination of C_p and free stream wind speed (i.e. $\overline{C_{pr}}$ with $U_{free}(H)$ or $\overline{C_{pl}}$ with $U_{free}(z)$). The other studies (where both C_p and U_{free} are clear) all use $\overline{C_{pr}}$ with $U_{free}(z)$. Thus, this common bias (23 of 27 studies) caused by using $\overline{C_{pr}}$ with $U_{free}(z)$ needs to be assessed.

Scenario 2: $\overline{C_{pr}}$ is defined using pressure and wind profiles from wind tunnel or CFD studies. If the wind profile in building energy models have systematic differences compared to the wind profile used to derive the pressure coefficients, then using the unmodified $\overline{C_{pr}}$ data will cause systematic errors in predicted pressure values (Fig. 1b). $\overline{C_{pl}}$ is calculated with the wind speed at the same height as the wind pressure, so is not a function of the wind profile [4,24], and is directly applicable in BES with a different wind profile from the one used to derive $\overline{C_{pl}}$ in the wind tunnel or CFD study. However, this does not apply to $\overline{C_{pr}}$ because it is based on the wind speed at a reference height [55,56]. For example, it is possible for different wind profiles to have the same wind speed at the reference height H. Neglecting differences in vertical wind profiles can cause biases. Potentially, this is a large problem as $\overline{C_{pr}}$ is widely used (Tables 1 and 2), and wind profiles in BES are normally different from the C_p source experiment wind profiles especially when using the

secondary sources (11 of 27 studies in Table 2). When the wind profiles for both the $\overline{C_{pr}}$ source and the BES are known, the $\overline{C_{pr}}$ data can be modified appropriately.

Scenario 3: If BES are combined with urbanised wind speed from urban canopy models, the free stream wind C_p values should be also accounted for the influence of the surrounding buildings (Fig. 1c). With increasing attention on urbanization and the impact of urban climate on building performance, efforts have been made to integrate BES with urban land surface or canopy models, such as combining EnergyPlus with Surface Urban Energy and Water Balance Scheme (SUEWS) [57–59] and the Vertical City Weather Generator (VCWG) [60]. Urban canopy models can modify meteorological variables to better account for the impact of buildings on local climate which will influence wind pressure calculation. For example, SUEWS provides a mean neighbourhood vertical profile of wind speed [58,61]. This differs from the undisturbed wind used in Eqs. (1) and (2) which are default weather data inputs in EnergyPlus. In this case, C_p values need to be corrected if the local wind speed is used (Fig. 1c). This has been largely overlooked in existing urban-building coupling energy simulation studies (e.g., use of C_p for surrounded case and disturbed local wind speed as reviewed by Ref. [62]).

The objectives of this study are to: (1) quantify the bias arising from using inconsistent reference height and wind pressure coefficient combinations; (2) assess the bias arising from the inconsistency of approaching wind profiles between BES and the source deriving the wind pressure coefficients; and (3) discuss the correction of wind pressure coefficients when combining building energy simulation tools and urban climate models.

2. Methods

To analyse the use of wind pressure coefficients in building energy simulation (BES), we use the BES tool EnergyPlus v9.4 [63] with Airflow Network (AFN) for ventilation rate calculation, and urban land surface model SUEWS [57,64] to simulate urban wind profiles. The wind pressure coefficient (C_p) data are obtained from the Tokyo Polytechnic University's aerodynamic database for low-rise buildings [25] under isolated and surrounded scenarios.

A two-storey reference building (Fig. 2a) based on ASHRAE Case 600 [65] is simulated for the Shanghai weather conditions in 2018 (SUEWS outputs forced with ERA5 [66]) for three settings:

(1) a rural, isolated (Fig. 2a)
(2) a neighbourhood with plan area fraction $\lambda_P = 0.3$ (Fig. 2b)
(3) a neighbourhood with plan area fraction $\lambda_P = 0.6$ (Fig. 2c).

Each floor of the building has a 3 m $\times$ 2 m window on the north and south facing walls, of which the upper 1/3 area hinged and openable to 20° for cross ventilation. For consistency with weather data, the building envelope thermal characteristics are set using the current local Shanghai building code [67]. This has overall heat transfer coefficients (U-values) of 0.39 W m^{-2} K^{-1} for the roof, 0.54 W m^{-2} K^{-1} for the external wall, 0.46 W m^{-2} K^{-1} for the floor, and 1.77 W m^{-2} K^{-1} for the windows. All windows are assumed to have 15% openable area and a discharge coefficient (C_d) of 0.61.

We calculate the natural ventilation rate, indoor overheating risk and energy saving potential. For the naturally ventilated mode, all windows are always open. The overheating risk is assessed using the Category II Chinese adaptive thermal model comfort corresponding to 75% satisfaction [68]. For the southern zone (i.e., applicable for Shanghai) the upper (T_{max}) and lower temperature limits (T_{min}) are [68]:

$$\begin{cases} T_{max} = 0.73 T_{rm} + 12.72 \ (18°C \leq T_{max} \leq 30°C) \\ T_{min} = 0.91 T_{rm} - 3.69 \ (16°C \leq T_{min} \leq 28°C) \end{cases} \tag{3}$$

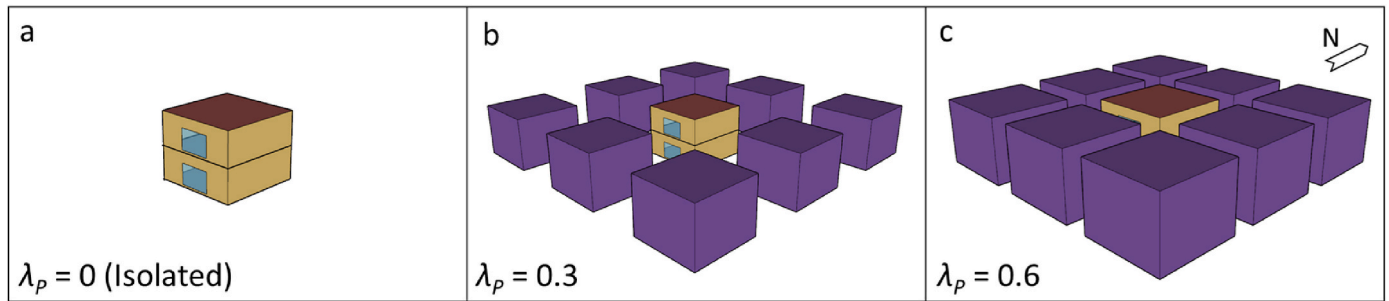where the running mean outdoor temperature T_{rm} is:

Fig. 2. A reference building (8 m (L) × 8 m (W) × 6.4 m (H)) is simulated using EnergyPlus in: (a) a rural (isolated) site, and in neighbourhoods with a plan area fractions $\lambda_P =$ (b) 0.3 and (c) 0.6.

$$T_{rm} = (1-k)\left(T_{od-1} + kT_{od-2} + k^2 T_{od-3} \cdots + k^6 T_{od-7}\right) \tag{4}$$

where k is a constant between 0 and 1, with 0.8 used as recommended [69], and T_{od-n} is the daily mean outdoor temperature n days ago (°C).

The air-conditioning mode follows the Code for Thermal Design of Civil Building recommendation of heating (18 °C) and cooling (26 °C) setpoints [70]. Windows can be open if air-conditioning is off and outdoor temperature is lower than indoor temperature. The cooling energy saving is calculated as the difference between the energy demand in hybrid mode (natural ventilation together with air conditioning) and fully air-conditioned mode.

The indoor overheating metrics are hours and degree hours exceeding the upper limits of temperatures (T_{max}) [71]. Local outdoor weather data required for EnergyPlus simulations for the two neighbourhoods are generated using SUEWS with the vertical profiles option of air temperature, relative humidity, and wind speed [58]. Air temperature and wind profiles evaluations using observations at three sites have reasonable accuracy [58,61]. For the neighbourhood cases, solar shading and inter-building external longwave radiative exchanges are also considered [72].

The normalised mean bias error (nMBE) assessment metric is used to compare two cases (x; y) for each of the three scenarios (Section 1, Fig. 1):

$$nMBE = \frac{1}{N} \frac{\sum_{i=1}^{N}(y_i - x_i)}{\overline{x_i}} \bullet 100\% \tag{6}$$

where x_i is the results from a consistent combination of C_p and level of U, and y_i is the results from the inconsistent combination of these for each hour i in the year (total of N = 8760 h). The ASHRAE-14 Guideline [73] acceptable uncertainty limits for building energy simulation programmes is the nMBE needs to be within ±10% for hourly data.

3. Results

3.1. $\overline{C_{pl}}$ & $U_{free}(z)$ vs $\overline{C_{pr}}$ & $U_{free}(z)$ for an isolated building

First, we need to derive a relation between surface averaged C_{pl} ($\overline{C_{pl}}$) and C_{pr} ($\overline{C_{pr}}$). To obtain the surface averaged C_p over the facet one can either calculate C_p at several locations and average, or define $\overline{C_{pl}}$ as the constant value that gives the correct total wind pressure over the facet [4]. The latter is analogous to Santiago and Martilli's [74] approach used for vertically distributed drag modelling of urban canopies, where the surface-averaged drag coefficient is the value giving the correct total drag over the building facet.

Akins and Cermak [4] suggested the differences between these two techniques are minimal, so we assume surface averaged C_p calculated with both methods are the same. We take the correct total wind pressure approach, which is defined by rearranging Eq. (1) or Eq 2 for $P_w(z)$ and integrating over the facet. For the pressure coefficient defined with velocity at the local opening height (Eq. (3)) one finds:

$$\overline{C_{pl}} = \frac{\int_0^H P_w(z)dz}{\int_0^H 0.5\rho U_{free}^2(z)dz} \tag{6}$$

and for the pressure coefficient defined with velocity at the building height (Eq. (1)) one finds:

$$\overline{C_{pr}} = \frac{\frac{1}{H}\int_0^H P_w(z)dz}{0.5\rho U_{free}^2(H)} \tag{7}$$

By only integrating over height it has been assumed that C_p variations in the horizontal can be neglected or that $P_w(z)$ has first been horizontally averaged across the facet. The approach is practical since velocity profiles in building energy models normally have vertical variation, so horizontal variation of C_p is not included.

To get the same average wind pressure over the building facet $\frac{1}{H}\int_0^H P_w(z)dz$, one can combine Eqs. (6) and (7) so that:

$$\overline{C_{pl}} \bullet \frac{1}{H}\int_0^H 0.5\rho U_{free}^2(z)dz = \overline{C_{pr}} \bullet 0.5\rho U_{free}^2(H) \tag{8}$$

which after rearranging becomes:

$$\overline{C_{pl}} = \overline{C_{pr}} \bullet \frac{0.5\rho U_{free}^2(H)}{\frac{1}{H}\int_0^H 0.5\rho U_{free}^2(z)dz} = \overline{C_{pr}} \bullet \frac{U_{free}^2(H)}{\frac{1}{H}\int_0^H U_{free}^2(z)dz} \tag{9}$$

To find $\overline{C_{pl}}$, values for $\overline{C_{pr}}$ and an equation for the wind speed are required. $\overline{C_{pr}}$ data from the TPU [25] database are used. Commonly in wind tunnel experiments (e.g. Ref. [25], a power law is used to describe the undisturbed wind speed at height z):

$$U_{free}(z) = U_{ref}\left(\frac{z}{z_{ref}}\right)^\alpha \tag{10}$$

where U_{ref} is the reference wind speed at height z_{ref} defined within the experiment, and the exponent α is an empirically derived coefficient. The vertically averaged wind speed is given by:

$$\frac{1}{H}\int_0^H U_{free}^2(z)dz = \frac{1}{H}\int_0^H \left(U_{ref}\left(\frac{z}{z_{ref}}\right)^\alpha\right)^2 dz = \frac{U_{ref}^2 H^{2\alpha}}{z_{ref}^{2\alpha}(2\alpha+1)} \tag{11}$$

Substituting Eqs. (10) and (11) into Eq. (9):

$$\overline{C_{pl}} = \overline{C_{pr}}\frac{U_{ref}^2\left(\frac{H}{z_{ref}}\right)^{2\alpha}}{\frac{U_{ref}^2 H^{2\alpha}}{z_{ref}^{2\alpha}(2\alpha+1)}} = \overline{C_{pr}}(2\alpha+1) \tag{12}$$

Using Eq. (12) with $\overline{C_{pr}}$ data from the TPU database (vertical profiles of original C_{pr} data are shown in Supplementary Material Fig. SM.1a), the results for an isolated reference building are given in Table 3, as are the $\overline{C_{pl}}$ data. EnergyPlus is used with the power law velocity profile that is the same as in the wind tunnel experiment in the TPU database assuming a suburban terrain and an exponent α of 0.2. EnergyPlus

Table 3

Surface-averaged wind pressure coefficients based on the reference height H $(\overline{C_{pr}})$ and opening height z $(\overline{C_{pl}})$ by wind angle related to the facet (0° is when wind is normal to the facet). $\overline{C_{pr}}$ is obtained from the TPU [25] database. $\overline{C_{pl}}$ is calculated by substituting $\overline{C_{pr}}$ into Eq. (12).

	0°	45°	90°	135°	180°
$\overline{C_{pr}}$	0.66	0.35	−0.57	−0.56	−0.28
$\overline{C_{pl}}$	0.92	0.49	−0.80	−0.79	−0.40

simulations are conducted for Shanghai in 2018 under naturally ventilated and mechanical cooling/heating modes as described in Section 2. The normalised mean bias errors (nMBE) for the ventilation rate, indoor overheating risks and cooling/heating energy demand are calculated between $\overline{C_{pl}}$ & $U_{free}(z)$ and $\overline{C_{pr}}$ & $U_{free}(z)$.

The $\overline{C_{pr}}$ with $U_{free}(z)$ underpredicts the annual air change per hour (ACH) ventilation rate (Fig. 3), with a nMBE of −15.5% (i.e., exceeding the ASHRAE-14 acceptable limit of ±10%). The annual overheating hours and degree hours are overpredicted by 11.9% and 12.9%, respectively. Such differences in overheating are found to largest during three consecutive heatwave days (13–15 July 2018, Fig. 4). During this period the $\overline{C_{pr}}$ & $U_{free}(z)$ case overpredicts the overheating hours and degree hours by 19.5% and 12.4%, respectively. Given the smaller ventilation rate, the nMBE in cooling energy saving is −10.5%, again exceeding the ASHRAE-14 limit. This suggests confusing $\overline{C_{pl}}$ with $\overline{C_{pr}}$ should be avoided when modelling ventilation rates and indoor overheating risks of naturally ventilated buildings, as well as the resultant cooling energy saving.

3.2. C_{pr} with wind profiles: wind tunnel vs outdoor

Swami and Chandra [24] and Akins et al. [5] suggest $\overline{C_{pl}}$ is not a function of the wind profile given it is based on the wind at the opening height z, which is the same as pressure measurement height. After further testing (section SM.2), the results suggest that $\overline{C_{pl}}$ independence on wind profile exponent α is acceptable.

However, $\overline{C_{pr}}$ obviously depends on the wind profile. Therefore, when the wind profile in the building energy simulation is different from the wind tunnel experiment where the C_p data are derived, $\overline{C_{pl}}$ can be used directly without further corrections. If only undisturbed wind speed at height H is available (e.g., TMY (typical meteorological year)
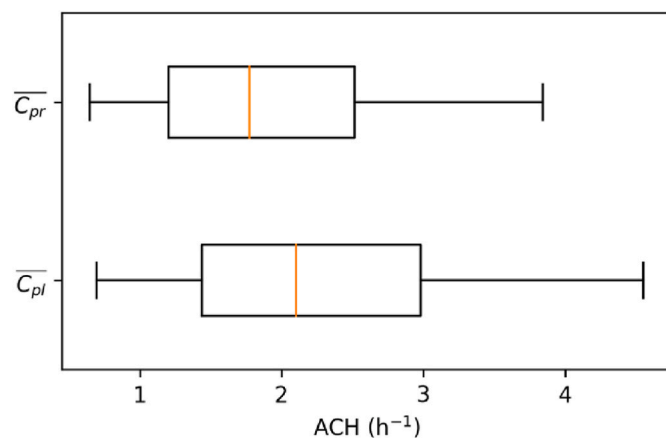

Fig. 3. Distribution of annual ACH (air change per hour, N = 8760) calculated with surface averaged wind pressure coefficients based on the opening height z $(\overline{C_{pl}})$ and reference height H $(\overline{C_{pr}})$, with interquartile range (box), median (orange line) and 5th and 95th percentiles (whiskers). (For interpretation of the references to colour in this figure legend, the reader is referred to the Web version of this article.)

wind speed data at 10 m), the $\overline{C_{pr}}$ values should be corrected. The EnergyPlus outdoor wind profile module determines the approaching wind speed profile $U(z)$ as [20]:

$$U(z) = U_{met} \left(\frac{\delta_{met}}{z_{met}} \right)^{\alpha_{met}} \left(\frac{z}{\delta} \right)^{\alpha} \tag{13}$$

It is calculated with the wind speed measured at a meteorological station U_{met} (i.e., weather data input). Standard World Meteorological Organisation (WMO) wind speed measurement height (z_{met}) is 10 m above ground level [75]. δ refers to the height where the vertical gradient of wind speed is assumed to become constant [58]. Typical values are given in Ref. [20] for different terrain types. For an isolated building in open country terrain $\alpha = \alpha_{met} = 0.14$ and $\delta = \delta_{met} = 270$ m.

Following Eq. (8), assuming $\overline{C_{pl}}$ data from the TPU database can be used directly (i.e. $\overline{C_{pl,WT}} = \overline{C_{pl,EP}}$) the average wind pressure on the building facet (Fig. 4) is calculated as

$$\frac{1}{H}\int_0^H P_w(z)dz = \overline{C_{pl,WT}} \bullet \frac{0.5\rho}{H}\int_0^H U_{EP}^2(z)dz = \overline{C_{pr,EP}} \bullet 0.5\rho U_{EP}^2(H) \tag{14}$$

and upon rearranging one finds

$$\overline{C_{pr,EP}} = \overline{C_{pl,WT}} \bullet \frac{\frac{1}{H}\int_0^H U_{EP}^2(z)dz}{U_{EP}^2(H)} \tag{15}$$

And similar to Eq. (12):

$$\overline{C_{pl,WT}} = \overline{C_{pr,WT}}(2\alpha_{WT}+1) \tag{16}$$

$$\overline{C_{pr,EP}} = \frac{\overline{C_{pl,WT}}}{2\alpha_{EP}+1} = \overline{C_{pr,WT}} \bullet \frac{2\alpha_{WT}+1}{2\alpha_{EP}+1} \tag{17}$$

where $\overline{C_{pr,EP}}$ and $\overline{C_{pl,EP}}$ are used with the EnergyPlus wind speed (U_{EP}), and $\overline{C_{pr,WT}}$ and $\overline{C_{pl,WT}}$ are obtained from the wind tunnel experiment.

To quantify the bias from neglecting the impact of vertical wind profile on C_{pr}, we model the isolated reference building in EnergyPlus, and calculate the ventilation rate, indoor overheating risks and cooling energy demand with both modified $\overline{C_{pr,EP}}$ and unmodified $\overline{C_{pr,WT}}$ obtained from the TPU database directly (Table 4). In the TPU database the wind profile exponent is $\alpha_{WT} = 0.2$. The default EnergyPlus wind profiles exponents (α_{EP}) are 0.14, 0.22 and 0.33, for open, rough and urban terrain [20], respectively.

Results (Fig. 5) show there are biases if an unmodified $\overline{C_{pr,WT}}$ is used along with varying α_{EP}. When $\alpha_{EP} < \alpha_{WT}$, $\overline{C_{pr,WT}}$ is smaller than $\overline{C_{pr,EP}}$, hence the ventilation rate is underpredicted when using $\overline{C_{pr,WT}}$. At $\alpha_{EP} = 0.14$, the nMBE in ACH is −4.5%, which is within the acceptable range of ASHRAE-14. The annual indoor overheating hours and degree hours are overpredicted by 2.3% and 3.7%, respectively. During the heatwave (13–15 July 2018) the overpredictions slightly increase to 8.0% and 4.4%. nMBE in cooling energy saving is −3.3%. With $\alpha_{EP} = 0.22$ and 0.33, the ventilation rates are overpredicted resulting in underpredicted overheating risks and overpredicted cooling energy saving (Fig. 5). Although all the biases are smaller than the ±10% ASHRAE-14 limit, they would increase in rougher terrain as the wind profile exponent increases.

3.3. Wind pressure coefficients for urban climate models

When local outdoor weather data are derived from urban weather/ climate models, the influence of the neighbourhood buildings are considered, but when calculating building facet wind pressure an 'undisturbed' flow is assumed in Eqs. (1) and (2). For example in SUEWS, the horizontally averaged neighbourhood wind speed is calculated for the roughness sublayer (RSL) based on a modified MOST (Monin–Obukhov similarity theory) approach [61]. Similar methods are used in other models like the Vertical City Weather Generator [60]. The
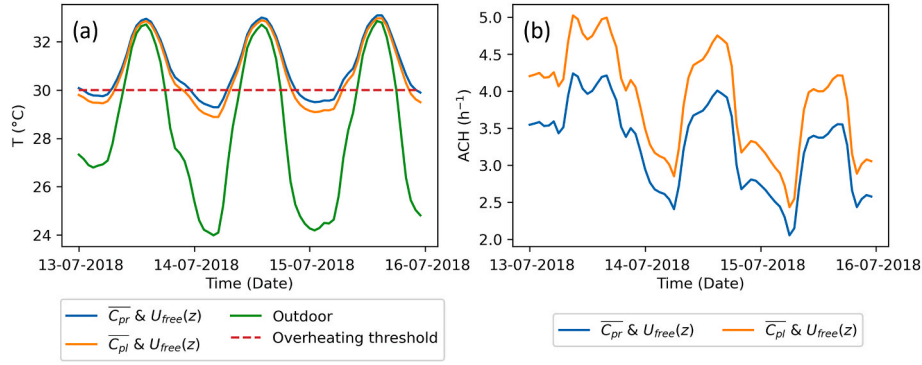
Fig. 4. Diurnal changes during three-day heatwave (13–15 July 2018) period in Shanghai for the upper floor (Fig. 2a) (a) indoor air temperatures, and (b) ventilation rates in ACH when calculated using the $\overline{C_{pl}}$ and $\overline{C_{pr}}$. i.e., $\overline{C_{pl}}$ & $U_{free}(z)$ vs $\overline{C_{pr}}$ & $U_{free}(z)$.

Table 4

Surface-averaged wind pressure coefficients from the wind tunnel experiment ($\overline{C_{pr,WT}}$) [25] and corrected with Eq. (17) ($\overline{C_{pr,EP}}$). The wind angles are relative to the surface (0° refers to wind blowing perpendicular to the facet).

	α	0°	45°	90°	135°	180°
$\overline{C_{pr,WT}}$	0.2	0.66	0.35	−0.57	−0.56	−0.28
$\overline{C_{pr,EP}}$	0.14	0.72	0.38	−0.62	−0.61	−0.31
	0.22	0.64	0.34	−0.55	−0.54	−0.27
	0.33	0.56	0.30	−0.48	−0.47	−0.24

advantages of using RSL wind are in calculating convective heat transfer on building surfaces and single-sided ventilation. But the cross-ventilation calculation will be biased if the urbanised wind speed is not used with corrected C_p values.

In SUEWS, the undisturbed wind profile can be modelled with an open rural setting (U_r), and the disturbed RSL wind profile can be modelled using different urban settings (U_u). To get the average wind pressure across the building facade:

$$\frac{1}{H}\int_0^H P_w(z)dz = \overline{C_{pl,WT}} \bullet \frac{0.5\rho}{H}\int_0^H U_r^2(z)dz = \overline{C_{pl,u}} \bullet \frac{0.5\rho}{H}\int_0^H U_u^2(z)dz \quad (18)$$

$$\overline{C_{pl,u}} = \overline{C_{pl,WT}} \bullet \frac{\int_0^H U_r^2(z)dz}{\int_0^H U_u^2(z)dz} \quad (19)$$

where $\overline{C_{pl,u}}$ is the corrected wind pressure coefficient for use alongside with the RSL wind (U_u) assuming the vertical profiles of U_u and U_r have the power law format of Eq. (13). Details of obtaining power law vertical profiles of U_u and U_r applicable for use with EnergyPlus are given in

Ref. [58]. Eq. (19) can be re-written as:

$$\overline{C_{pl,u}} = \overline{C_{pl,WT}} \bullet \frac{U_r^2(10)H^{2\alpha_r}\delta_u^{2\alpha_u}(2\alpha_u+1)}{U_u^2(10)H^{2\alpha_u}\delta_r^{2\alpha_r}(2\alpha_r+1)} \quad (20)$$

Since the RSL wind have lower velocities than the undisturbed wind, $\overline{C_{pl,WT}}$ values need to be scaled to larger magnitudes ($\overline{C_{pl,u}}$) to obtain the same wind pressure. To quantify the biases of using the disturbed RSL wind speed U_u with $C_{pl,WT}$, we consider two idealised neighbourhoods with aligned buildings in EnergyPlus with plan area fractions of $\lambda_P = 0.3$ and 0.6, with the surface-averaged C_p values given in Table 5 (original $C_{pr,WT}$ vertical profiles are shown in Fig. SM.1b, c).

For the neighbourhood with a λ_P of 0.3, using $\overline{C_{pl,WT}}$ with the RSL wind $U_u(z)$ largely underpredicts the ventilation rate, with an annual nMBE of −19.0%, exceeding the ASHRAE-14 acceptable uncertainty limits. The annual indoor overheating hours and degree hours are overpredicted by 5.9% and 13.2%, respectively. During the heatwave

Table 5

Surface-averaged wind pressure coefficients from the wind tunnel experiment ($\overline{C_{pr,WT}}$) [25], calculated with Eq. (12) ($\overline{C_{pl,WT}}$) and corrected with Eq. (20) ($\overline{C_{pl,u}}$) for urbanised wind (U_u) for two plan area fractions ($\lambda_P = 0.3$ and 0.6) for different wind angles (0° refers to wind blows perpendicular to the facet).

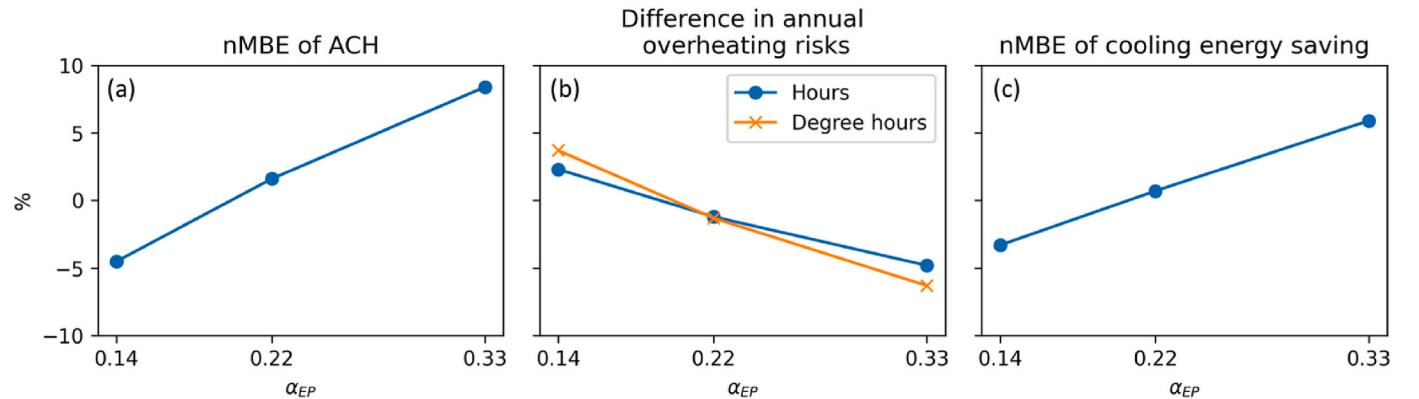|		0°	45°	90°	135°	180°
$\lambda_P = 0.3$	$\overline{C_{pr,WT}}$	0.15	0.05	−0.22	−0.24	−0.16
	$\overline{C_{pl,WT}}$	0.21	0.07	−0.31	−0.34	−0.22
	$\overline{C_{pl,u}}$	0.34	0.11	−0.51	−0.55	−0.37
$\lambda_P = 0.6$	$\overline{C_{pr,WT}}$	−0.13	−0.09	−0.17	−0.20	−0.21
	$\overline{C_{pl,WT}}$	−0.18	−0.13	−0.24	−0.28	−0.29
	$\overline{C_{pl,u}}$	−0.66	−0.46	−0.86	−1.02	−1.07

Fig. 5. Normalised mean bias errors (nMBE) linked to using unmodified $\overline{C_{pr,WT}}$ from the wind tunnel experiment compared to modified $\overline{C_{pr,EP}}$ for three EnergyPlus wind profiles exponents (α_{EP}) for (a) ventilation rate in ACH, (b) difference in annual overheating risks and (c) cooling energy saving.

(13–15 July 2018), the indoor overheating hours difference is 0, because in both cases the indoor air temperature exceeds the maximum temperature threshold throughout (Fig. 6a), but the overprediction in degree hours increases to 18.4%. The nMBE in cooling energy saving is −14.0%.

Additionally, the ventilation rate is simulated with $\overline{C_{pl,WT}}$ and the free stream wind $U_r(z)$ to evaluate Eq. (18). Results (Fig. 7), as expected, suggest that using $\overline{C_{pl,WT}}$ with $U_r(z)$ and $\overline{C_{pl,u}}$ with $U_u(z)$ give very similar results (nMBE = 0.8%). The small differences are possibly due to the buoyancy-driven ventilation dominating, since the wind speed input to EnergyPlus is also used for calculations of both convection and indoor air temperature.

Generally for the $\lambda_P = 0.6$ neighbourhood, the biases are slightly smaller (cf. $\lambda_P = 0.3$) because of the lower wind speeds. The nMBE for the ventilation rate is −16.2%, while the annual indoor overheating hours and degree hours are overpredicted by 4.7% and 9.0%, respectively. However, during the heatwave (Fig. 6b) when ventilation rates are small, differences in overheating hours become 20.3%. The nMBE in cooling energy saving is −9.6%.

In summary, when modelling naturally ventilated buildings using urbanised wind speeds, correcting the C_p data correspondingly is important. Increasing λ_P can lead to slightly smaller annual biases, but during heatwaves when the natural ventilation rates are small, larger biases can be seen.

4. Discussion

There are various assumptions and approximations made for C_p to simplify the calculation of wind pressure on building facets that can cause various uncertainties. Some of these have been assessed previously, such as those linked to the surface averaged values and different data sources [76,77]. Most common sources of C_p data provide surface averaged values based on the reference height ($\overline{C_{pr}}$), rather than being based on the opening height ($\overline{C_{pl}}$). Given the definition (Eq. (7)), $\overline{C_{pr}}$ data needs to be corrected in some circumstances, but this appears to have been overlooked in most existing studies. In this study we explore three scenarios to quantify biases from inconsistent combination of C_p value
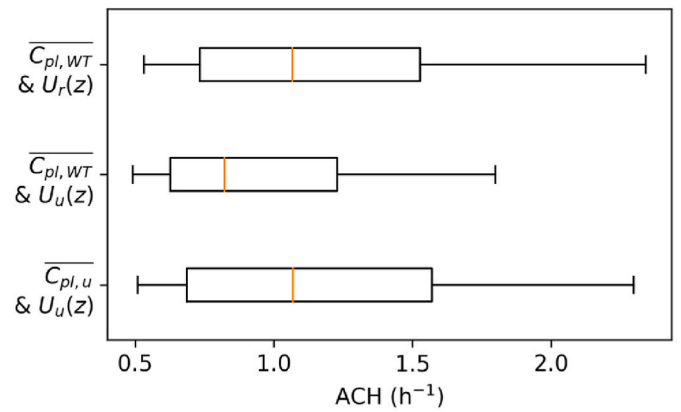

Fig. 7. As Fig. 3, but for modelling ventilation rate (as ACH) with three combinations of $\overline{C_{pl}}$ and $U(z)$. $\overline{C_{pl,WT}}$ & $U_r(z)$ and $\overline{C_{pl,u}}$ & $U_u(z)$ give the similar results but vary slightly due to differences in buoyancy-driven ventilation, whereas assuming $\overline{C_{p,WT}}$ & $U_u(z)$ is inconsistent and therefore biased.

and wind speed.

In each scenario we find critical differences, which impact the resulting predictions especially of ventilation rates and indoor overheating risks for naturally ventilated buildings. These findings confirm that natural ventilation rate calculations are sensitive to the C_p and wind data used. Notably, we revise the relation between the $\overline{C_{pr}}$ and $\overline{C_{pl}}$ that has often been neglected in building energy simulations. Our results demonstrate the importance of modifying C_p data for wind conditions, including the wind speed height, wind profile and terrain surface type (e.g. extensive grass – 'undisturbed', neighbourhoods at different λ_P – 'disturbed' or 'urbanised').

There are limitations in our work. Although surface averaged C_p data are widely used, their errors (cf. local C_p data) are assumed to be relatively smaller if openings are located in the facet centre instead of edges where extreme values occur [76]. Hence, we only consider windows located in the centre of each facet. We consider only one climate type, but expect that relative results should be similar across different
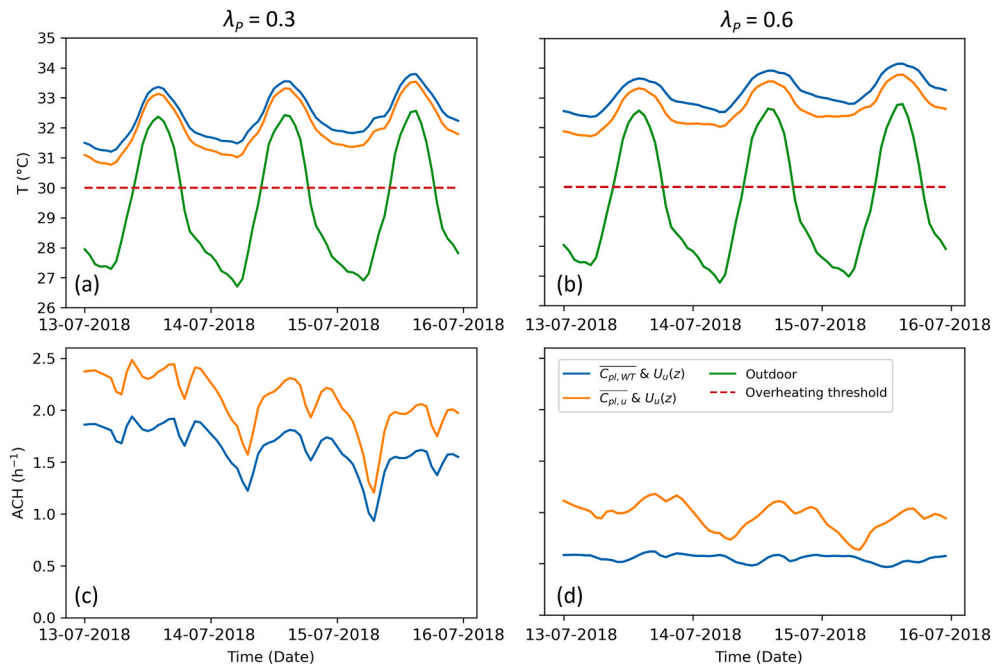

Fig. 6. As Fig. 4, but using surface-averaged wind pressure coefficients from wind tunnel experiments ($\overline{C_{pl,WT}}$) [25] and corrected with Eq. (20) ($\overline{C_{pl,u}}$) at for two neighbourhoods when λ_P is (a, c) 0.3 and (b, d) 0.6, for (a, b) air temperature and (c, d) ventilation rate in ACH.

climates, as found by Ref. [77]. Future work could evaluate a wider range of climates and different building geometries (e.g., gable and hip roofs).

5. Conclusions

Wind pressure coefficients are widely used in building energy simulations (BES) to calculate the ventilation rate. However, wind pressure coefficients may be used inappropriately given their assumptions and simplifications. Users obtain them from datasets that most commonly have a fixed *reference* height H (hereafter C_{pr}) but some use a *local* opening height z (hereafter C_{pl}). From analysis of three typical scenarios, we conclude these impacts are critical especially when simulating natural ventilation rates, indoor overheating and cooling energy saving. By using surface averaged C_{pr} ($\overline{C_{pr}}$) data in BES directly in Shanghai climate, biases can potentially lead to:

(1) if using free stream wind speed at z in EnergyPlus, rather than the velocity at H
   - nMBE = −15.5% in predictions of ventilation rate, 11.9% for indoor overheating hours and 12.9% for overheating degree hours, and −10.5% for cooling energy saving
(2) if using wind profiles that differ from the wind tunnel and CFD studies used to derive the pressure coefficients
   - relatively small errors (nMBE of ventilation rate of up to 8.4%), but these may increase when there are greater differences between wind tunnel experiment and BES wind profile exponents
(3) if using urbanised wind speeds, but $\overline{C_{pr}}$ is calculated based on free stream wind speeds
   - large errors in ventilation rates (nMBE of up to −19.0%), indoor overheating risks (differences in annual hours and degree hours of up to 5.9% and 13.2%, respectively) and cooling energy saving (nMBE of up to −14.0%) when two different neighbourhoods ($\lambda_P = 0.3$ and 0.6) are considered.

Furthermore, all of these biases increase during heatwave periods.

Clearly these biases should be considered when simulating the impact of natural ventilation using building energy simulation tools. To improve the accuracy of natural ventilation rate prediction in BES we recommend:

- C_p data should be used with the free stream wind speed at a consistent height, i.e. reference height H for $\overline{C_{pr}}$, or local opening height z for $\overline{C_{pl}}$. For power law wind profiles, $\overline{C_{pr}}$ and $\overline{C_{pl}}$ can be inter-converted with Eq. (12).
- As the wind profile in BES could be different from the ones in wind tunnel and CFD studies where $\overline{C_{pr}}$ are derived, care is needed with which C_p data are used. $\overline{C_{pl}}$ this can be used directly, but not for $\overline{C_{pr}}$ data. The latter should be corrected based on wind profiles in the BES and the wind tunnel/CFD studies (e.g., Eq. (17)).
- When BES use urbanised wind speed (i.e., not 'undisturbed'), C_p data should be corrected to account for the relation between undisturbed free stream and urbanised wind (Eq. (19)).

CRediT authorship contribution statement

Xiaoxiong Xie: Writing – review & editing, Writing – original draft, Visualization, Resources, Methodology, Investigation. **Zhiwen Luo:** Writing – review & editing, Supervision, Methodology, Funding acquisition, Conceptualization. **Sue Grimmond:** Writing – review & editing, Supervision, Funding acquisition. **Lewis Blunn:** Writing – review & editing, Investigation.

Declaration of competing interest

The authors declare that they have no known competing financial interests or personal relationships that could have appeared to influence the work reported in this paper.

Data availability

Information on the data underpinning the results presented here can be found at https://doi.org/10.5281/zenodo.7543153 (Xie et al., 2023).

Appendix A. Supplementary data

Supplementary data to this article can be found online at https://doi.org/10.1016/j.buildenv.2022.109951.

References

[1] U.S. Department of Energy, Chapter 13: alternative modeling processes, in: EnergyPlus Version 9.4.0 Documentation: Engineering Reference, 2020, pp. 601–705.
[2] Integrated Environmental Solutions, MacroFlo Calculation Methods [WWW Document], 2018. URL, https://help.iesve.com/ve2018/, 6.30.22.
[3] TRNSYS, TRNSYS 17: Mathematical Reference, 2009.
[4] R.E. Akins, J.E. Cermak, Wind Pressure on Buildings, Colorado State University, 1976.
[5] R.E. Akins, J.A. Peterka, J.E. Cermak, Averaged pressure coefficients for rectangular buildings, in: Zement-Kalk-Gips, 1979, pp. 369–380.
[6] V. Costanzo, R. Yao, T. Xu, J. Xiong, Q. Zhang, B. Li, Natural ventilation potential for residential buildings in a densely built-up and highly polluted environment. A case study, Renew. Energy 138 (2019) 340–353.
[7] Z. Luo, J. Zhao, J. Gao, L. He, Estimating natural-ventilation potential considering both thermal comfort and IAQ issues, Build. Environ. 42 (2007) 2289–2298.
[8] Z. Tan, X. Deng, Assessment of natural ventilation potential for residential buildings across different climate zones in Australia, Atmosphere 8 (2017) 177.
[9] L. Yang, G. Zhang, Y. Li, Y. Chen, Investigating potential of natural driving forces for ventilation in four major cities in China, Build. Environ. 40 (2005) 738–746.
[10] J. Lim, Y. Akashi, R. Ooka, H. Kikumoto, Y. Choi, A probabilistic approach to the energy-saving potential of natural ventilation: effect of approximation method for approaching wind velocity, Build. Environ. 122 (2017) 94–104.
[11] B. Park, S. Lee, Investigation of the energy saving efficiency of a natural ventilation strategy in a multistory school building, Energies 13 (2020), 2020 1746 13, 1746.
[12] R. Ramponi, I. Gaetani, A. Angelotti, Influence of the urban environment on the effectiveness of natural night-ventilation of an office building, Energy Build. 78 (2014) 25–34.
[13] T. Schulze, U. Eicker, Controlled natural ventilation for energy efficient buildings, Energy Build. 56 (2013) 221–232.
[14] C. Heracleous, A. Michael, Assessment of overheating risk and the impact of natural ventilation in educational buildings of Southern Europe under current and future climatic conditions, Energy 165 (2018) 1228–1239.
[15] A. Mavrogianni, M. Davies, J. Taylor, Z. Chalabi, P. Biddulph, E. Oikonomou, P. Das, B. Jones, The impact of occupancy patterns, occupant-controlled ventilation and shading on indoor overheating risk in domestic environments, Build. Environ. 78 (2014) 183–198.
[16] C. Schünemann, D. Schiela, R. Ortlepp, How window ventilation behaviour affects the heat resilience in multi-residential buildings, Build. Environ. 202 (2021), 107987.
[17] F. Stazi, E. Tomassoni, C. Di Perna, Super-insulated wooden envelopes in Mediterranean climate: summer overheating, thermal comfort optimization, environmental impact on an Italian case study, Energy Build. 138 (2017) 716–732.
[18] U.J. Sung, S. Cho, D.H. Seo, K.D. Song, Analysis of reduced cooling load for a multistorey-building incorporating a ventilated double skin façade with a solar chimney channel, Int. J. Vent. 11 (2013) 381–391.
[19] M. Sadeghi, G. Wood, B. Samali, R. de Dear, Effects of urban context on the indoor thermal comfort performance of windcatchers in a residential setting, Energy Build. 219 (2020), 110010.
[20] ASHRAE, ASHRAE Handbook : Fundamentals, American Society of Heating, Refrigerating and Air-Conditioning Engineers, Atlanta, 2005.
[21] D. Cóstola, B. Blocken, J.L.M.L.M. Hensen, Overview of pressure coefficient data in building energy simulation and airflow network programs, Build. Environ. 44 (2009) 2027–2036.
[22] M. Liddament, Air Infiltration Calculation Techniques: an Applications Guide, Coventry, 1986.

[23] DesignBuilder, DesignBuilder V7 Help [WWW Document], 2022. URL, https://designbuilder.co.uk/helpv7.0/index.htm, 11.21.22.

[24] M.V. Swami, S. Chandra, Procedures for Calculating Natural Ventilation Airflow Rates in Buildings, Cape Canaveral, 1987.

[25] TPU, Aerodynamic Database for Low-Rise Buildings, 2007 (Tokyo, Japan).

[26] J. Axley, Multizone airflow modeling in Buildings: history and theory, HVAC R Res. 13 (2007) 907–928.

[27] A. Belleri, R. Lollini, S.M. Dutton, Natural ventilation design: an analysis of predicted and measured performance, Build. Environ. 81 (2014) 123–138.

[28] U.S. Department of Energy, EnergyPlus Version 9.4.0 Documentation: Input Output Reference, 2020.

[29] EnergyPlus, GitHub - NREL/EnergyPlus [WWW Document], 2022. URL, https://github.com/NREL/EnergyPlus, 7.18.22.

[30] J.M. Gimenez, F. Bre, N.M. Nigro, V. Fachinotti, Computational modeling of natural ventilation in low-rise non-rectangular floor-plan buildings, Build. Simulat. 11 (2018) 1255–1271.

[31] A. Toesca, D. David, A. Kuster, M. Lussault, K. Johannes, An urban thermal tool chain to simulate summer thermal comfort in passive urban buildings, Build. Environ. 215 (2022), 108987.

[32] A. Botti, M. Leach, M. Lawson, N.S. Hadjidimitriou, Developing a meta-model for early-stage overheating risk assessment for new apartments in London, Energy Build. 254 (2022) 111586.

[33] F. Bre, J.M. Gimenez, A cloud-based platform to predict wind pressure coefficients on buildings, Build. Simulat. 15 (2022) 1507–1525.

[34] W. Guo, S. Liang, W. Li, B. Xiong, H. Wen, Combining EnergyPlus and CFD to predict and optimize the passive ventilation mode of medium-sized gymnasium in subtropical regions, Build. Environ. 207 (2022), 108420.

[35] UrbaWind, URBAWIND | the Urban Wind Modeling Software - METEODYN [WWW Document], 2022. URL, https://meteodyn.com/business-sectors/microclimate-and-urban-planning/13-urba-wind.html, 7.18.22.

[36] T. Dogan, P. Kastner, Streamlined CFD simulation framework to generate wind-pressure coefficients on building facades for airflow network simulations, Build. Simulat. 14 (2021) 1189–1200.

[37] J. Saif, A. Wright, S. Khattak, K. Elfadli, Keeping cool in the desert: using wind catchers for improved thermal comfort and indoor air quality at half the energy, Buildings 11 (2021) 100.

[38] N.R.M. Sakiyama, L. Mazzaferro, J.C. Carlo, T. Bejat, H. Garrecht, Natural ventilation potential from weather analyses and building simulation, Energy Build. 231 (2021), 110596.

[39] J. Song, X. Huang, D. Shi, W.E. Lin, S. Fan, P.F. Linden, Natural ventilation in London: towards energy-efficient and healthy buildings, Build. Environ. 195 (2021), 107722.

[40] D.P. Albuquerque, N. Mateus, M. Avantaggiato, G. Carrilho da Graça, Full-scale measurement and validated simulation of cooling load reduction due to nighttime natural ventilation of a large atrium, Energy Build. 224 (2020), 110233.

[41] B. Raji, M.J. Tenpierik, R. Bokel, A. van den Dobbelsteen, Natural summer ventilation strategies for energy-saving in high-rise buildings: a case study in The Netherlands, Int. J. Vent. 19 (2020) 25–48.

[42] N.T. Bayraktar, V. Ok, Numerical evaluation of the effects of different types of shading devices on interior occupant thermal comfort using wind tunnel experimental data, Build. Simulat. 12 (2019) 683–696.

[43] B. Belmans, D. Aerts, S. Verbeke, A. Audenaert, F. Descamps, Set-up and evaluation of a virtual test bed for simulating and comparing single- and mixed-mode ventilation strategies, Build. Environ. 151 (2019) 97–111.

[44] D. Kim, S.J. Cox, H. Cho, J. Yoon, Comparative investigation on building energy performance of double skin façade (DSF) with interior or exterior slat blinds, J. Build. Eng. 20 (2018) 411–423.

[45] C.A. Short, J. Song, L. Mottet, S. Chen, J. Wu, J. Ge, Challenges in the low-carbon adaptation of China's apartment towers, Build. Res. Inf. 46 (2018) 899–930.

[46] R.G. Southall, An assessment of the potential of supply-side ventilation demand control to regulate natural ventilation flow patterns and reduce domestic space heating consumption, Energy Build. 168 (2018) 201–214.

[47] T. Van Nguyen, F. De Troyer, New surrogate model for wind pressure coefficients in a schematic urban environment with a regular pattern, Atmosphere 9 (2018) 113.

[48] B. Knoll, J. Phaff, W. de Gids, Pressure coefficient simulation program, Air Infiltration Rev 17 (1996) 1–5.

[49] F. Bre, A.S. Silva, E. Ghisi, V.D. Fachinotti, Residential building design optimisation using sensitivity analysis and genetic algorithm, Energy Build. 133 (2016) 853–866.

[50] M.J. Sorgato, A.P. Melo, R. Lamberts, The effect of window opening ventilation control on residential building energy consumption, Energy Build. 133 (2016) 1–13.

[51] J. Joe, W. Choi, H. Kwon, J.H. Huh, Load characteristics and operation strategies of building integrated with multi-story double skin facade, Energy Build. 60 (2013) 185–198.

[52] W. You, M. Qin, W. Ding, Improving building facade design using integrated simulation of daylighting, thermal performance and natural ventilation, Build. Simulat. 6 (2013) 269–282.

[53] G. Carrilho Da Graça, N.R. Martins, C.S. Horta, Thermal and airflow simulation of a naturally ventilated shopping mall, Energy Build. 50 (2012) 177–188.

[54] E.L. Olsen, Q. Chen, Energy consumption and comfort analysis for different low-energy cooling systems in a mild climate, Energy Build. 35 (2003) 560–571.

[55] C. Fang, B.L. Sill, Pressure distribution on a low-rise building model subjected to a family of boundary layers, J. Wind Eng. Ind. Aerod. 56 (1995) 87–105.

[56] W. Yang, Y. Quan, X. Jin, Y. Tamura, M. Gu, Influences of equilibrium atmosphere boundary layer and turbulence parameter on wind loads of low-rise buildings, J. Wind Eng. Ind. Aerod. 96 (2008) 2080–2092.

[57] L. Järvi, C.S.B. Grimmond, A. Christen, The surface urban energy and water balance Scheme (SUEWS): evaluation in Los Angeles and Vancouver, J. Hydrol. 411 (2011) 219–237.

[58] Y. Tang, T. Sun, Z. Luo, H. Omidvar, N. Theeuwes, X. Xie, J. Xiong, R. Yao, S. Grimmond, Urban meteorological forcing data for building energy simulations, Build. Environ. 204 (2021), 108088.

[59] X. Xie, Z. Luo, S. Grimmond, T. Sun, Predicting Natural Ventilation Potential in Idealised Urban Neighbourhoods across Chinese Climate Zones, Prep, 2022.

[60] M. Moradi, E.S. Krayenhoff, A.A. Aliabadi, A comprehensive indoor–outdoor urban climate model with hydrology: the Vertical City Weather Generator (VCWG v2.0.0), Build. Environ. 207 (2022), 108406.

[61] N.E. Theeuwes, R.J. Ronda, I.N. Harman, A. Christen, C.S.B. Grimmond, Parametrizing horizontally-averaged wind and temperature profiles in the urban roughness sublayer, Boundary-Layer Meteorol. 173 (2019) 321–348.

[62] F. Johari, G. Peronato, P. Sadeghian, X. Zhao, J. Widén, Urban building energy modeling: state of the art and future prospects, Renew. Sustain. Energy Rev. 128 (2020), 109902.

[63] U.S. Department of Energy, Chapter 1: overview, in: EnergyPlus Version 9.4.0 Documentation: Engineering Reference, 2020, pp. 20–24.

[64] H.C. Ward, S. Kotthaus, L. Järvi, C.S.B. Grimmond, Surface urban energy and water balance Scheme (SUEWS): development and evaluation at two UK sites, Urban Clim. 18 (2016) 1–32.

[65] ANSI/ASHRAE, Standard Method of Test for the Evaluation of Building Energy Analysis Computer Programs, 2011 (\).

[66] H. Hersbach, B. Bell, P. Berrisford, S. Hirahara, A. Horányi, J. Muñoz-Sabater, J. Nicolas, C. Peubey, R. Radu, D. Schepers, A. Simmons, C. Soci, S. Abdalla, X. Abellan, G. Balsamo, P. Bechtold, G. Biavati, J. Bidlot, M. Bonavita, G. De Chiara, P. Dahlgren, D. Dee, M. Diamantakis, R. Dragani, J. Flemming, R. Forbes, M. Fuentes, A. Geer, L. Haimberger, S. Healy, R.J. Hogan, E. Hólm, M. Janisková, S. Keeley, P. Laloyaux, P. Lopez, C. Lupu, G. Radnoti, P. de Rosnay, I. Rozum, F. Vamborg, S. Villaume, J.N. Thépaut, J. Muñoz-Sabater, J. Nicolas, C. Peubey, R. Radu, D. Schepers, A. Simmons, C. Soci, S. Abdalla, X. Abellan, G. Balsamo, P. Bechtold, G. Biavati, J. Bidlot, M. Bonavita, G. Chiara, P. Dahlgren, D. Dee, M. Diamantakis, R. Dragani, J. Flemming, R. Forbes, M. Fuentes, A. Geer, L. Haimberger, S. Healy, R.J. Hogan, E. Hólm, M. Janisková, S. Keeley, P. Laloyaux, P. Lopez, C. Lupu, G. Radnoti, P. Rosnay, I. Rozum, F. Vamborg, S. Villaume, J. N. Thépaut, The ERA5 global reanalysis, Q. J. R. Meteorol. Soc. 146 (2020) 1999–2049.

[67] MoHURD, Design Standard for Energy Efficiency of Public Buildings (GB50189-2015), Ministry of Housing and Urban-rural Development, P.R. China, Beijing, 2015.

[68] MoHURD, Evaluation Standard for Indoor Thermal Environment in Civil Buildings (GB/T50785-2012), Ministry of Housing and Urban-rural Development, P.R. China, Beijing, 2012.

[69] J.F. Nicol, M.A. Humphreys, Adaptive thermal comfort and sustainable thermal standards for buildings, Energy Build. 34 (2002) 563–572.

[70] MoHURD, Code for Thermal Design of Civil Building (GB50176-2016), Ministry of Housing and Urban-rural Development, P.R. China, Beijing, 2016.

[71] S.M. Porritt, P.C. Cropper, L. Shao, C.I. Goodier, Ranking of interventions to reduce dwelling overheating during heat waves, Energy Build. 55 (2012) 16–27.

[72] X. Xie, Z. Luo, S. Grimmond, T. Sun, W. Morrison, Impact of inter-building longwave radiative exchanges on building energy performance and indoor overheating, Build. Environ. 209 (2022), 108628.

[73] ASHRAE, ASHRAE Guideline 14: Measurement of Energy, Demand, and Water Savings, 2014 (Atlanta).

[74] J.L. Santiago, A. Martilli, A dynamic urban canopy parameterization for mesoscale models based on computational fluid dynamics Reynolds-averaged Navier–Stokes microscale simulations, Boundary-Layer Meteorol. 137 (2010) 417–439.

[75] WMO, Guide to Meteorological Instruments and Methods of Observation, WMO, Geneva, 2017.

[76] D. Cóstola, B. Blocken, M. Ohba, J.L.M. Hensen, Uncertainty in airflow rate calculations due to the use of surface-averaged pressure coefficients, Energy Build. 42 (2010) 881–888.

[77] R. Ramponi, A. Angelotti, B. Blocken, Energy saving potential of night ventilation: sensitivity to pressure coefficients for different European climates, Appl. Energy 123 (2014) 185–195.